doi:10.1016/S0022-2836(02)01472-9 *J. Mol. Biol.* (2003) **326**, 1189–1201

JMB

Available online at www.sciencedirect.com

SCIENCE DIRECT®

Solution Structure of the Cytotoxic RNase 4 from Oocytes of Bullfrog *Rana catesbeiana*

Chun-Hua Hsu[1,2], You-Di Liao[1]*, Yun-Ru Pan[1], Lih-Woan Chen[1] Shih-Hsiung Wu[2,3], Ying-Jen Leu[1,4] and Chinpan Chen[1]*

[1]*Institute of Biomedical Sciences, Academia Sinica Taipei 115, Taiwan, ROC*

[2]*Institute of Biochemical Sciences, National Taiwan University, Taipei 106, Taiwan ROC*

[3]*Institute of Biological Chemistry, Academia Sinica Taipei 115, Taiwan, ROC*

[4]*Department of Life Science National Tsing-Hua University Hsin-Chu 300, Taiwan, ROC*

**Corresponding authors*

Cytotoxic ribonucleases with antitumor activity are mainly found in the oocytes and early embryos of frogs. Native RC-RNase 4 (RNase 4), consisting of 106 residues linked with four disulfide bridges, is a cytotoxic ribonuclease isolated from oocytes of bullfrog *Rana catesbeiana*. RNase 4 belongs to the bovine pancreatic ribonuclease (RNase A) superfamily. Recombinant RC-RNase 4 (rRNase 4), which contains an additional Met residue and glutamine instead of pyroglutamate at the N terminus, was found to possess less catalytic and cytotoxic activities than RNase 4. Equilibrium thermal and guanidine-HCl denaturation CD measurements revealed that RNase 4 is more thermally and chemically stable than rRNase 4. However, CD and NMR data showed that there is no gross conformational change between native and recombinant RNase 4. The NMR solution structure of rRNase 4 was determined to comprise three α-helices and two sets of antiparallel β-sheets. Superimposition of each structure with the mean structure yielded an average root mean square deviation (RMSD) of 0.72(±0.14) Å for the backbone atoms, and 1.42(±0.19) Å for the heavy atoms in residues 3–105. A comparison of the 3D structure of rRNase 4 with the structurally and functionally related cytotoxic ribonuclease, onconase (ONC), showed that the two H-bonds in the N-terminal pyroglutamate of ONC were not present at the corresponding glutamine residue of rRNase 4. We suggest that the loss of these two H-bonds is one of the key factors responsible for the reductions of the conformational stability, catalytic and cytotoxic activities in rRNase 4. Furthermore, the differences of side-chain conformations of subsite residues among RNase A, ONC and rRNase 4 are related to their distinct catalytic activities and base preferences.

Keywords: antitumor; cytotoxicity; ribonuclease; NMR; solution structure

Introduction

Several ribonucleases have been isolated from bullfrog *Rana catesbeiana*[1,2] and they all belong to the bovine pancreatic ribonuclease (RNase A) superfamily, based on the conserved residues involved in catalytic activity. These frog enzymes are composed of 105–111 amino acid residues linked with four disulfide bridges, and possess different catalytic activities and base preferences. Among the four disulfide-bridges, the frog ribonucleases lack the disulfide bridge that corresponds to that of RNase A Cys65-Cys72, and have instead a different novel bridge near their C termini. In addition to their ribonucleolytic activity, these ribonucleases are also cytotoxic toward tumor cells, similar to onconase (ONC) isolated

Abbreviations used: RNase A, bovine pancreatic ribonuclease; RNase 4, native RC-RNase 4 from oocytes of *Rana catesbeiana*; rRC-RNase 4, recombinant RC-RNase 4; ONC, the ribonuclease, onconase, isolated from oocytes of *Rana pipiens*; BS-RNase, bovine seminal ribonuclease from bull semen; RI, ribonuclease inhibitor; RC-RNase, frog ribonuclease from oocytes of *R. catesteiana*; hRNase, human ribonucleases; IPTG, isopropyl-β-thiogalactopyranoside; GdnHCl, guanidine-HCl; CD, circular dichroism; NOE, nuclear Overhauser enhancement; NOESY, nuclear Overhauser enhancement spectroscopy; DQF-COSY, double-quantum-filtered scalar-correlated spectroscopy; TOCSY, total correlation spectroscopy; RMSD, root mean square deviation; CSI, chemical shift index.

E-mail addresses of the corresponding authors: ydliao@ibms.sinica.edu.tw; bmchinp@ccvax.sinica.edu.tw

0022-2836/03/$ - see front matter

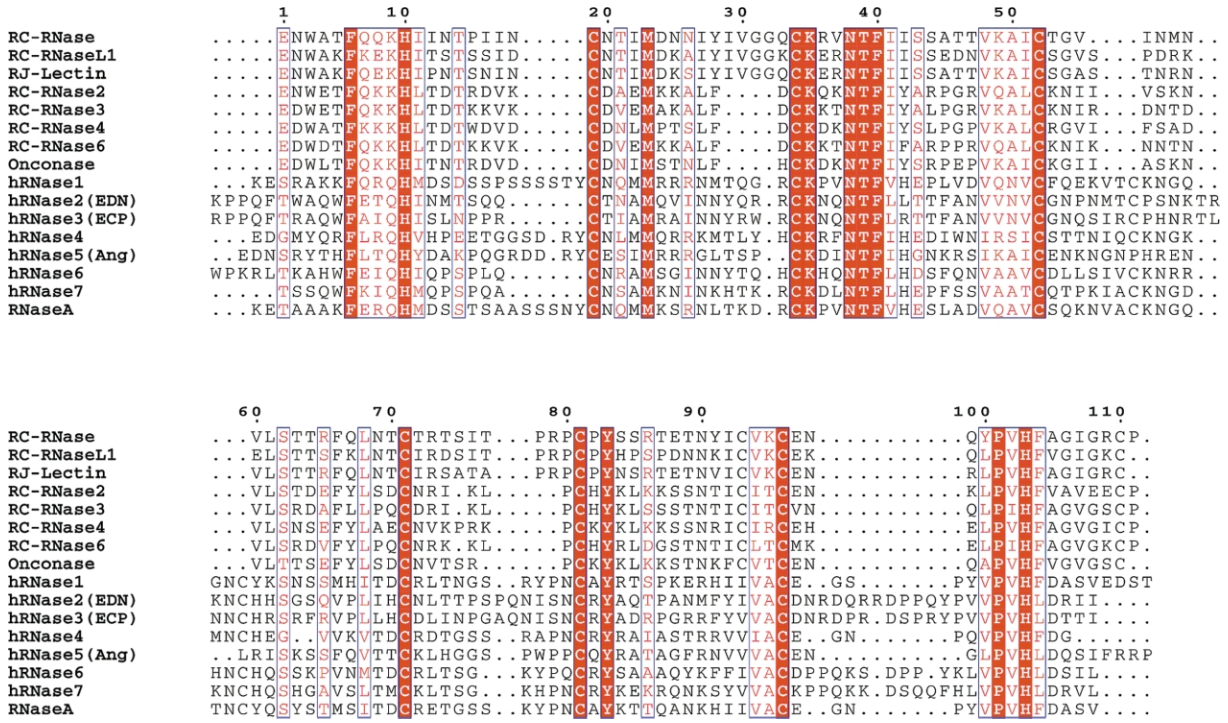

Figure 1. Sequence alignments of frog ribonucleases, human ribonucleases and bovine pancreatic ribonuclease (RNase A). RC-RNase L1 is a ribonuclease isolated from the liver of bullfrog *Rana catesbeiana*, and RJ-Lectin is a lectin from *Rana japonica*. The sequence number on the top is based on the sequence of RC-RNase and the alternate name of hRNase2, hRNase3 and hRNase5, respectively, is shown in parentheses.

from frog *Rana pipiens*.[3] ONC is currently undergoing phase III clinical trial as an antitumor drug.[4] Another unique characteristic of frog ribonucleases is that they all contain a pyroglutamate residue at the N terminus and that this N-terminal pyroglutamate plays an important role in catalytic and cytotoxic activity.[5] In contrast, the N-terminal pyroglutamate of human ribonuclease 5 (hRNase 5), also called angiogenin, is not associated with catalytic activity.[6] How ribonuclease mediates cytotoxicity has been extensively studied[7–9] and there are three critical properties involved in ribonuclease cytotoxicity: (i) the ribonuclease must be active in RNA catalysis since cytotoxic ribonucleases affect cell death by catalyzing the cleavage of cellular RNA; (ii) the ribonuclease must be stable, e.g. ONC has an unusually high denaturation temperature of ~90 °C at pH 6.0, much higher than that of non-cytotoxic RNase A ($t_m = 63$ °C at pH 6.0);[7] (iii) the ribonuclease must be able to evade ribonuclease inhibitor (RI). RNase A exhibits a high affinity with RI ($K_i \sim 10^{-14}$ M) and is not cytotoxic, despite its relatively high ribonucleolytic activity, 500 times more effective than ONC.[10] Similar to RNase A, human pancreatic ribonuclease (hRNase 1) also possesses high enzymatic activity and extreme sensitivity to RI. Accordingly, it is not cytotoxic. In contrast, ONC and bovine seminal ribonuclease (BS-RNase) from bull semen[11] shows a very weak affinity with RI, and its cytotoxicity is attributed to its ability to evade RI. On the basis of the complex structure of porcine RI and RNase A,[12] RNase A variants with decreasing affinities for RI have been designed and studied. These variants have been shown to retain their catalytic activities in the presence of RI, and were found to be cytotoxic to a transformed cell line.[7] Recently, a similar approach was applied to hRNase 1, which can be rendered toxic to human cancer cells by replacing several amino acid residues in its sequence.[13]

To date, a number of structures of RNase A and its complexes have been solved using X-ray crystallographic or NMR methods.[12,14–19] The structures of five human ribonucleases have also been solved: hRNase 1[20]; EDN (hRNase 2)[21]; ECP (hRNase 3);[22,23] hRNase 4,[24] and angiogenin (hRNase 5).[25] In addition, the complex of human RI and angiogenin has been reported.[26] Although a relatively large number of 3D structures of the members in the RNase A superfamily have been determined, only a few of these ribonucleases possess cytotoxicity toward tumor cells. For example, studies involving frog cytotoxic ribonucleases only include the determination of the X-ray crystal structure of ONC[27] and NMR solution structures of RC-RNase.[28] Thus, to gain insight into structure/function relationship and to investigate the possibility of using frog ribonuclease as a potential agent for tumor therapy, more detailed structural studies on frog cytotoxic ribonucleases are needed. RC-RNase 4 (RNase 4), one of the cytotoxic ribonucleases isolated from

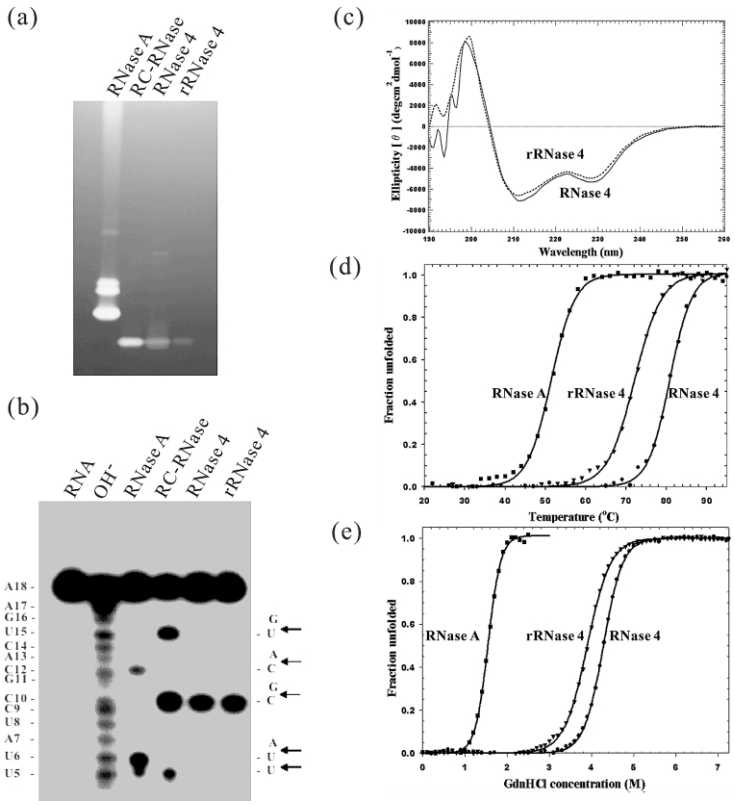

Figure 2. (a) *Zymogram*. RNaseA (20 ng), RC-RNase (20 ng), RNase 4 (200 ng) and rRNase 4 (200 ng) were loaded onto 13.3% RNA-casting SDS-PAGE and assayed for their activities. (b) Base specificity. An 18-mer 5′end-labeled RNA was partially digested with RNase A (1 ng), RC-RNase (4 ng), RNase 4 (0.6 μg) and rRNase 4 (9 μg), respectively, and subjected to 8 M urea-15% PAGE separation and autoradiography. OH indicates that the RNA substrate was treated with 0.05 M sodium bicarbonate–carbonate at pH 9.2 and 90 °C for four minutes. The RNA sequence and cleavage sites are shown in the left and right margins, respectively. (c) Comparison of CD spectra of 20 μM rRNase 4 and RNase 4 in 20 mM phosphate buffer at pH 3.0. (d) Equilibrium CD titration experiments as a function of temperature for rRNase 4, RNase 4, and RNase A. (e) Equilibrium CD titration experiments as a function of GdnHCl concentration for rRNase 4, RNase 4, and RNase A. Equilibrium unfolding titration CD experiments clearly demonstrate that both RNase 4 and rRNase 4 were more stable than RNase A thermally and chemically.

oocytes of *Rana catesbeiana*, is composed of 106 amino acid residues. The sequence alignment of RNase 4 with several other ribonucleases is shown in Figure 1. Amino acid sequence analysis on frog ribonucleases indicates that RNase 4 is very similar to ONC. However, the base preference of RNase 4 is CpG, whereas that of ONC is UpG. Here, using CD and heteronuclear multidimensional NMR methods, we studied the conformational stability and determined the high-resolution 3D solution structure of rRNase 4. By comparing our rRNase 4 structure to those of ONC and RNase A, the structure–function relationships are discussed.

Results

Catalytic properties

The catalytic activity of RNase A, RC-RNase, RNase 4 and rRNase 4 were assayed by zymogram on an RNA-casting SDS-PAGE (Figure 2(a)). Results showed that RNase A was the most active, then RC-RNase, RNase 4 and rRNase 4 in descending order. The relative activity of these ribonucleases toward yeast total RNA was measured by the acid-insoluble method. The catalytic activity of RNase 4 was 0.02% of that of RC-RNase, and

Table 1. Kinetic parameters of ribonucleases with dinucleotide as substrate

	CpG			UpG			
Enzymes ÿ	k_{cat} (min^{-1})	K_m (μM)	k_{cat}/K_m ($min^{-1}\,M^{-1}$)	k_{cat} (min^{-1})	K_m (μM)	k_{cat}/K_m ($min^{-1}\,M^{-1}$)	Specific activity[a] ($A/\mu g$)
RC-RNase	1311 ± 100	16 ± 1.5	$8.1 \times 10^7 \pm 2.7 \times 10^6$	2848 ± 419	27 ± 5	$1.1 \times 10^8 \pm 4.5 \times 10^6$	822 ± 48
RNase 4	22 ± 5.6	40 ± 2.6	$5.6 \times 10^5 \pm 2.3 \times 10^4$	39 ± 8	81 ± 19	$4.8 \times 10^5 \pm 1.2 \times 10^4$	0.13 ± 0.005
rRNase 4	1 ± 0.2	114 ± 29	$9.3 \times 10^3 \pm 201$	2.3 ± 0.6	285 ± 81	$8.1 \times 10^3 \pm 131$	0.01 ± 0.001

Assay of ribonuclease activity with dinucleotide as substrate was described in the text.
[a] Specific activity of ribonuclease was defined as the increase of absorbance in the soluble fraction at 260 nm at 37 °C for 15 minutes per μg of ribonuclease in 50 mM sodium acetate (pH 6.0).

that of rRNase 4 was 8% of that of RNase 4. The catalytic properties of these ribonucleases toward dinucleotides CpG and UpG were also determined by k_{cat}/K_m analysis as shown in Table 1. The values of RNase 4 for CpG and UpG were much less than those of RC-RNase, 150, 200-fold, respectively. Furthermore, the values of rRNase 4 for these two dinucleotides were also much less than that of RNase 4 in the aspect of K_m increase, three-four-fold, and k_{cat} decrease, 15–20-fold. The base specificities of these ribonucleases were further determined using an 18-mer 5′end-labeled RNA as substrate. Figure 2(b) shows that RNase 4 and rRNase 4 predominantly cleaved the CpG bond, while RC-RNase cleaved the CpG, UpG and UpU bond in descending order, and RNaseA predominantly cleaved UpA and CpA bond. These RNA sequencing results were in good agreement with the k_{cat}/K_m values toward dinucleotides as described above. In conclusion, the modification of the N-terminal pyroglutamate of RNase 4 markedly decreased its catalytic activity, but did not significantly affect its base specificity.

Cytotoxicity

To evaluate the potential for the use of RNase 4 in human tumor therapy, the cytotoxicity of this enzyme was determined for several cell lines including human leukemia K562 cells, human cervical carcinoma HeLa cells, human breast cancer MCF-7 cells, and bovine aortic endothelial cells BAEC. The IC_{50} of RNase 4 was 0.5 μM for K562 cells, 1 μM for HeLa cells, 1.5 μM for MCF-7 cells, and 0.3 μM for BAEC. Although RNase 4 has very low catalytic activity compared to that of RC-RNase, they have similar cytotoxic potential. In contrast, RNase A possesses high catalytic activity but does not possess cytotoxicity. However, with the disruption of hydrogen bonds contributed by N-terminal pyroglutamate in rRNase 4, its cytotoxicity was markedly decreased, with an IC_{50} of more than 8 μM. Therefore, the catalytic activity of ribonuclease may be essential but not sufficient for cytotoxicity, and the disruption of its N-terminal pyroglutamate may disrupt both catalytic and cytotoxic activities.

Conformational stability and secondary structure based on CD data

CD spectra of rRNase 4 at different pH values (pH 3.0–7.5) are very similar and indicate that its secondary structure is independent of change of pH. As shown in Figure 2(c), the CD spectra of RNase 4 and rRNase 4 are almost identical, indicating that their secondary structures are highly similar. Interestingly, RNase 4 and rRNase 4 displayed two negative ellipticities at 212 nm and 228 nm, while the CD spectra of other frog ribonucleases from *R. catesbeiana* only showed a single minimum at 211 nm (data not shown). The average content of the secondary structure of rRNase 4 estimated by using CONTIN-LL, SELCON3 and CDSSTR methods was 14.9% of the α-helix, 35.4% of the β-strand, 22.6% of the turn, and 27.8% of the unordered structure, respectively. t_m values of 81 °C and 72 °C were obtained for RNase 4 and rRNase 4, respectively, based on equilibrium titration experiments at different temperatures from 20 °C to 100 °C at pH 3.0, as shown in Figure 2(d). Further, equilibrium unfolding at different concentrations of guanidine-HCl (GdnHCl) shown in Figure 2(e) revealed that rRNase 4 possesses a smaller C_m value (3.9 M) than that (4.3 M) of native protein. For comparison, the t_m (52 °C) and C_m (1.6 M) of RNase A, both of which are much smaller than those of RNase 4 and rRNase 4, were also measured at pH 3.0.

Resonance assignment and secondary structure of rRNase 4

With high thermostability and well-dispersed NMR data, rRNase 4 is an excellent compound for NMR structural studies. Because CD data indicated that there is no global structural change for rRNase 4 at different pH values (pH 3.0–7.5), we therefore chose pH 3.5 for the structural study since under this condition NMR data are best behaved. Initially, NMR techniques were used to further examine the structural similarities between the native and recombinant proteins. Figure 3

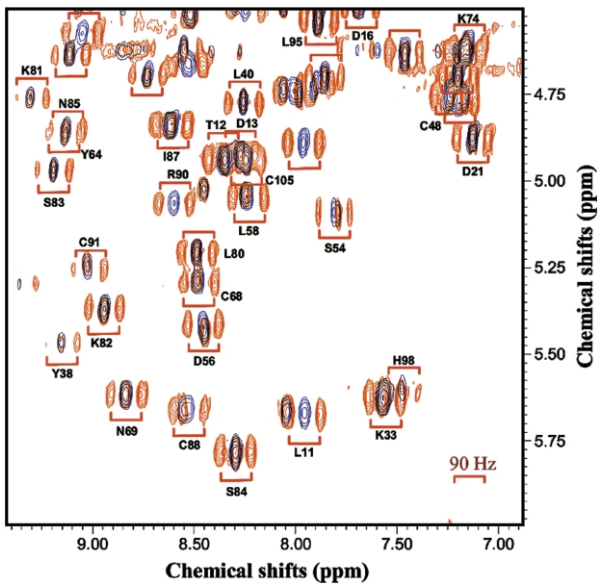

Figure 3. Superimposition of the fingerprint regions of two TOCSY spectra, one with ^{15}N decoupling and the other one without ^{15}N decoupling, for the sample containing both RNase 4 and ^{15}N-labeled rRNase 4 is shown. Each cross-peak of $H^N/C^\alpha H$ splitting into two peaks with a coupling constant of 90 Hz was observed for ^{15}N-labeled rRNase 4 in the experiment without decoupling and labeled. For clarity, only a partial region of the spectra is displayed.

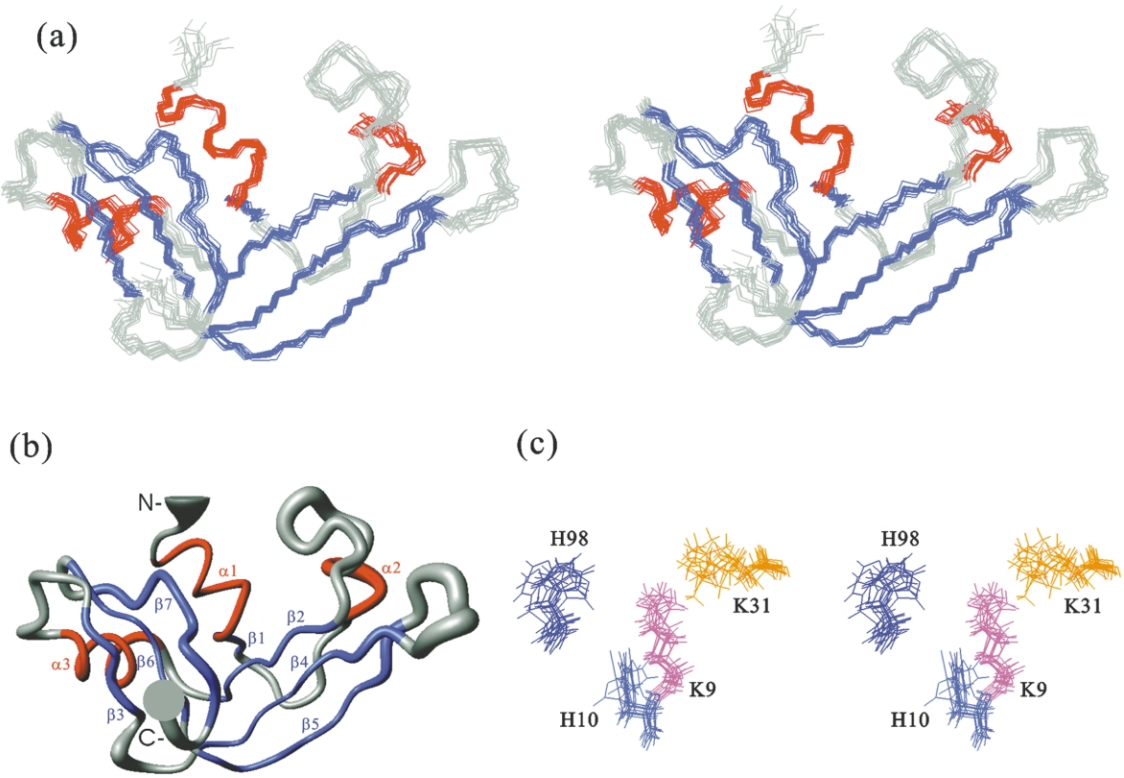

Figure 4. NMR solution structures of rRNase 4 obtained from simulated annealing and energy minimization calculations using the X-PLOR program. (a) Stereo view of the superimposition of the backbone (N, C^{α}, and C′) atoms of 15 NMR solution structures of rRNase 4. The structures are best fitted to residues 3–105. (b) The ribbon structure of the mean NMR solution structure of rRNase 4. A spline function was drawn through the C^{α} atoms and the radius of the cylindrical rod corresponds to the mean of the global displacements. (c) Stereo view of the superimposition of side-chain atoms of active site (P_1 subsite) residues of rNase 4. For clarity, the side-chain conformations of ten selected structures from 15 NMR structures are shown. RMSD values of these residues are: 1.21 Å, 1.19 Å, 1.68 Å, and 1.12 Å for Lys9, His10, Lys31, and His98, respectively.

shows the superimposition of the fingerprint regions of two total correlated spectroscopy (TOCSY) spectra, one with ^{15}N decoupling and the other one without ^{15}N decoupling, for the sample containing both RNase 4 and ^{15}N-labeled rRNase 4. Only a few residues have moderate shift changes between these two proteins and this finding indicates that RNase 4 and rRNase 4 exhibit very similar tertiary structure. ^{1}H, ^{13}C, and ^{15}N resonance assignments of rRNase 4 have been completely assigned and published.[29] On the basis of the summary of the NMR parameters, we determined that rRNase 4 contains three α-helices (Trp3-His10, Cys19-Leu22, and Pro41-Cys48) and seven β-strands (Leu11-Thr12, Lys33-Tyr38, Ala55-Leu58, Phe63-Val70, Tyr78-Asn85, Ile87-Glu92, and Leu95-Val102). Furthermore, according to the observed cross-over nuclear Overhauser effects (NOEs) between the β-strands and the slowly exchanging amide protons, these seven β-strands were further identified to form two antiparallel β-sheets. The medium intensity of the $d_{\alpha N}(i, i+3)$ NOE, along with the backbone ϕ, ψ angles of residues Phe28-Lys31 and Glu92-Leu95 based on the derived NMR structures described in the next paragraph, revealed that these two segments form type I′ β-turns. The segment of Cys48-Val51, however, exhibits a type II β-turn. All seven proline residues (Pro24, Pro41, Pro43, Pro72, Pro75, Pro96, and Pro106) were found to be *trans* conformations, due to the observation of strong $d_{\alpha\delta}(i, i+1)$ NOEs. To check the rigidity and to identify the hydrogen bonds, we carried out an amide-proton exchange study at pH 3.5, 310 K. We found that the residues with medium and slow amide proton exchange were all located in the well-defined regions by the NMR data, and that most of these amide protons formed characteristic hydrogen bonds in the secondary structure elements.

Structure description

For 3D structure determination, a set of 1323 restraints was applied for simulated annealing and energy minimization calculations. Among these restraints, 1130 were interproton distances; 92 were hydrogen bonds; 97 were torsional angles, and four were disulfide-bond restraints. A total of 15 structures were chosen to represent the ensemble of NMR structures on the basis of the lowest target function, and minimal distance and torsional angle restraint violations, in the final

Table 2. Structural statistics on the final set of simulated annealing structures of rRNase 4

A. *Constraints used*	
Distance restraints	
Intra-residue	339
Sequential	396
Medium-range	127
Long-range	268
Hydrogen bonds	46 × 2
Disulfide bonds	4
Total distance restraints	1226
Dihedral angles	
Backbone ϕ, φ	74
Sidechain χ^1	23
B. *Statistics for the final X-PLOR structures*	
Number of structures in the final set	15
X-PLOR energy (kcal/mol)	
E_{NOE}	20.70 ± 3.00
E_{cdih}	2.64 ± 0.64
$E_{bond} + E_{angle} + E_{improper}$	370.31 ± 12.7
E_{elec}	1.98 ± 0.07
E_{VDW}	170.28 ± 2.92
NOE violations	
Number > 0.5 Å	None
RMSD (Å)	0.024
Deviation from idealized covalent geometry	
Angle (deg.)	0.79 ± 0.01
Impropers (deg.)	0.47 ± 0.03
Bonds (Å)	0.005
Mean global r.m.s deviation (Å)	
Backbone (N, C^α, C′)	
Residues (secondary structure)	0.62 ± 0.13
Residues (3–105)	0.72 ± 0.14
Heavy atoms	
Residues (secondary structure)	1.27 ± 0.18
Residues (3–105)	1.42 ± 0.19
Ramachandran data	
Residues in most favored regions (%)	81.9
Residues in allowed regions (%)	18.1
Residues in generously allowed regions (%)	0
Residues in disallowed regions (%)	0

stage. All of these structures were consistent with both experimental data and standard covalent geometry, and displayed no violations greater than 0.5 Å for distance restraints. The solution structure of rRNase 4 is composed of three α-helices and two antiparallel β-sheets. Superposition of each structure with the mean structure yielded an average RMSD of 0.72(±0.14) Å for the backbone atoms (Figure 4(a) and (b)) and 1.42(±0.19) Å for the heavy atoms in residues 3–105. The RMSD for side-chain heavy atoms of each residue is in the range of 0.33–2.48 Å. Figure 4(c) shows the ensemble of side-chain conformation of the main active site (P_1) residues of Lys9, His10, Lys31, and His98 in rRNase 4, with the RMSD of 1.21 Å, 1.19 Å, 1.68 Å, and 1.12 Å, respectively. The structural statistics on the final set of structures are given in Table 2. Analysis of the ensemble of 15 structures using PROCHECK-NMR revealed that 81.9% of the residues lie in the most favored regions, and 18.1% of the residues lie in allowed regions, of the Ramachandran ϕ, ψ dihedral-angle plot (plot not shown). Two sets of dihedral angles were observed for the Cys19-Cys68 disulfide bond, with average angles of 107(±7)° (five structures) and −78(±12)° (ten structures), revealing that there are two different conformers in this disulfide bridge. The average dihedral angle of the other three disulfide bridges was 158(±8)° for Cys30-Cys76, 145(±5)° for Cys48-Cys91, and −109(±13)° for Cys88-Cys105. Therefore, the conformation of each of the four disulfide bridges appears to be very rigid, since precise dihedral angles were observed. Most of the hydrogen bonds in these 15 structures are located in the α-helix, β-sheet, and β-turn regions. In the type I′ β-turn region of Glu92-Leu95, as expected, the hydrogen bond of Glu92 CO/Leu95 NH was detected in all of the NMR structures. RNase 4 contains four arginine, 12 lysine, eight aspartic acid, and four glutamic acid charged residues. At neutral pH, RNase 4 carries an overall positive charge, which is distributed into two main regions. One region is composed of Lys7, Lys8, Lys9, and Lys31, and the other is composed of Lys71, Lys73, Lys74, Lys79, Lys81, and Lys82. Negative charged residues are distributed more randomly, and only one negative charged region was clearly observed, which contained Asp13, Asp16, Asp18, and Asp20.

Discussion

Although the catalytic and cytotoxic activities of rRNase 4 are markedly less than the native protein, CD and NMR data revealed that they possess very similar secondary and tertiary structures. RNase 4 possesses a distinct CD spectroscopic characteristic with two negative ellipticities at 212 nm and 228 nm compared to one (~211 nm) observed for other frog ribonucleases. A sequence comparison (Figure 1) reveals that RNase 4 contains a unique Trp residue at position 15. We therefore constructed and expressed the mutated protein W15A, in which Trp15 of rRNase 4 was replaced with Ala, and examined its biophysical properties. The CD spectrum of the W15A mutant showed only a negative ellipticity at ~211 nm, indicating that the ellipticity minimum at 228 nm is due to the effect of Trp15 indole ring. Compared to our RC-RNase structure derived using 2D ^{1}H NMR techniques,[28] we obtained many more unambiguous medium and long-range NOEs as well as dihedral angle restraints based on heteronuclear multidimensional NMR experiments for rRNase 4. As a result, NMR structures of rRNase 4 display higher quality and resolution than RC-RNase. As anticipated, the tertiary fold and secondary structures of rRNase 4 are similar to structures of the RNase A superfamily. Based on the 3D structure of rRNase 4, we found that the unusual chemical shifts observed in the Tyr78, Ser59, Asn34 and Ser39 residues of rRNase 4[29] correlated well with the 3D structure in four primary ways, described

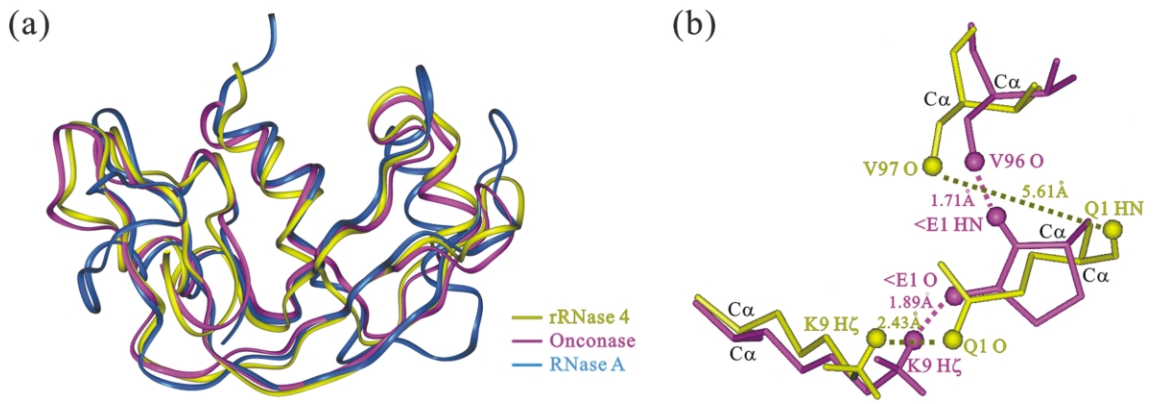

Figure 5. (a) Superimposition of the ribbon structure of rRNase 4, RNase A, and the structurally and functionally related cytotoxic ribonuclease, ONC. This diagram was generated using multiple-sequence alignment in the InsightII program. The RMSD for the coordinates of the C^{α} atoms used in the superimposition calculation between rRNase 4 and ONC is 1.25 Å and between rRNase 4 and RNase A is 2.18 Å. The atomic coordinates of RNase A and ONC were obtained from the Protein Data Bank with accession number 7RSA[51] and 1ONC,[27] respectively. (b) Conformational comparison between the N-terminal glutamine in rRNase 4 and the N-terminal pyroglutamate in ONC is shown. Two H-bonds observed in the N-terminal pyroglutamate of ONC (magenta) are not present in the corresponding glutamine residue of rRNase 4 (yellow).

as follows. (i) The side-chain of Tyr78 was completely buried within the interior of the folded protein, and thus four distinct resonances were observed. Interestingly, the equivalent residues, Tyr97 in RNase A, Tyr83 in RC-RNase, and Tyr77 in ONC, are all shielded from the solvent. In RNase A, the side-chain hydroxy group of Tyr97 was found to form a hydrogen bond to the main-chain oxygen of Lys41, which is a catalytically important residue. It is suggested that this H-bond may stabilize the *trans* isomer of the Lys41-Pro42 peptide bond and thereby lock the main chain of Lys41 into a position that maximizes catalysis. Accordingly, even though Tyr97 is remote from the active site, its side-chain contributes to catalysis.[30] However, this hydrogen bond was not consistently observed in our rRNase 4 structures. (ii) The observation of the labile hydroxy proton of Ser59 results from the H-bond formation between this OH group and the backbone amide proton of Ile87. This H-bond was present in all 15 NMR structures. The equivalent H-bond was also found in the corresponding residues of Thr59 and Phe86 in ONC, and of Ser75 and Ile106 in RNase A. (iii) The unusual chemical shifts of the side-chain amide protons of Asn34 are due to the aromatic ring current effect of Phe36. The motif of Asn34-Thr35-Phe36 in RNase 4 is conserved in the corresponding residues among all members of the RNase A superfamily. These unusual chemical shifts of the side-chain amide protons of Asn34 were also detected in our NMR structural studies involving two other frog ribonucleases, RC-RNase 2 and RC-RNase L1.[31,32] Therefore, it is likely that these unusual shifts are a common feature in the RNase A superfamily. (iv) The hydroxy group of Ser39 is shielded from the solvent in rRNase 4, and hence this labile resonance could be detected. In contrast, the equivalent Ser residues in ONC and RNase A are exposed to the aqueous phase. Therefore, the corresponding labile proton might not be detected in both ONC and RNase A.

To gain insight into the structure/function relationships, we superimposed ribbon structures of rRNase 4, ONC and RNase A using multiple-sequence alignment of the InsightII program (Figure 5(a)). The RMSD for the coordinates of the C^{α} atoms used in the superposition calculation between rRNase 4 and ONC and between rRNase 4 and RNase A is 1.25 Å and 2.18 Å, respectively. The main structural differences among these three proteins are seen at the loop regions. The N termini of rRNase 4 and RNase A are exposed in the aqueous phase, whereas the N terminus of ONC is folded against the N-terminal α-helix. Two H-bonds were observed in the pyroglutamate of ONC, but these two H-bonds were not detected in the N-terminal glutamine residue of rRNase 4, as shown in Figure 5(b). The loss of these two hydrogen bonds in rRNase 4 explains why the N terminus is highly exposed in the aqueous phase. Another interesting feature in the rRNase 4 structure is that the unique Trp15 forms a hydrophobic cluster with Tyr38 and Tyr64. This hydrophobic cluster may enhance the conformational stability in both RNase 4 and rRNase 4, and it may also cause the change in the orientation of N-terminal α-helix in rRNase 4 compared to that in ONC. Moreover, this hydrophobic cluster makes the loop region near Trp15 more rigid than expected. Comparison of the surface structures showed that RNase A contains a cluster of positive charges at the active site region. This finding indicates that the charge distribution may be an important factor in catalytic activity since RNase A possesses a much higher catalytic activity than rRNase 4 and ONC.

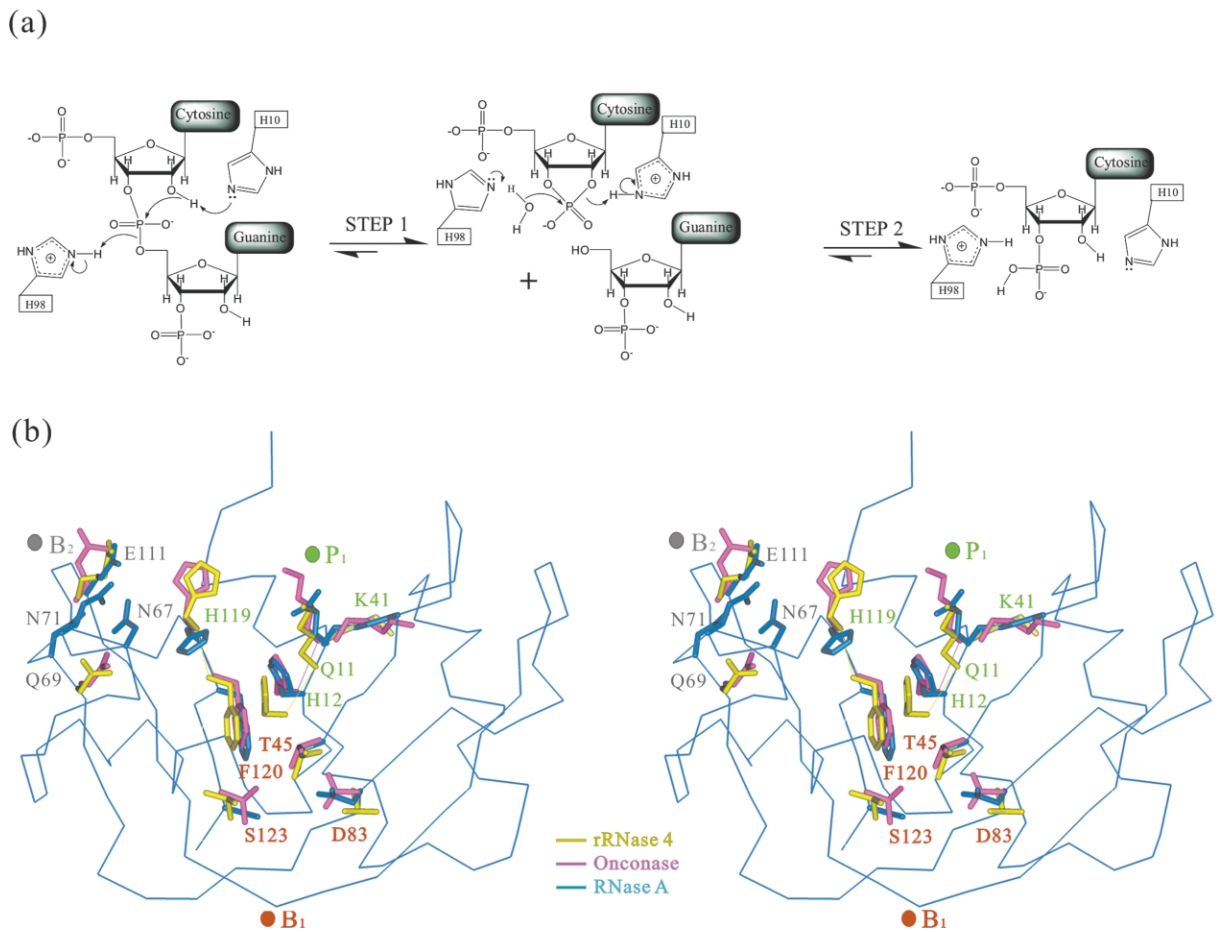

Figure 6. (a) Putative mechanism for the transphosphorylation (STEP 1) and hydrolysis reactions (STEP 2) catalyzed by rRNase 4. (b) Comparison of side-chain conformations of P_1, B_1, and B_2 site residues of RNase A and of the corresponding residues in rRNase 4 and ONC. The C^{α} heavy atom structure was generated based on RNase A structure. The side-chain conformations of subsites of rRNase 4, ONC, and RNase A are shown in yellow, magenta, and blue, respectively. The locations of P_1, B_1, and B_2 subsites are indicated and the residues in each subsite are labeled in green, red, and gray, respectively.

Based on the generally accepted two-step catalytic reaction mechanism of RNase A,[33,34] the putative catalytic mechanism of rRNase 4 was generated and is shown in Figure 6(a). In the first step of transphosphorylation reaction, His10 acts as a general base that abstracts a proton from the 2′-OH of cytidine and thereby facilitates the attack of the 2′-oxygen on the phosphorus atom. Next, His98 acts as a general acid that protonates the 5′-oxygen of guanosine to facilitate the displacement of guanine nucleoside and a 2′,3′-cyclic phosphodiester intermediate is formed. In the subsequent step, His10 and His98 reverse their roles, that is, His10 acts as a general acid and His98 as a general base and the intermediate is hydrolyzed by a water molecule within the active site to form a 3′ monophosphate ester as the final product. The important residues in the subsites (P_1, B_1, and B_2) of RNase A in catalytic reaction have been identified.[35,36] In the P_1 subsite (active site), the three main catalytic residues, His12, Lys41, and His119, are conserved in all members of the RNase A superfamily. The role of the two His residues in catalysis is described above. In contrast, Lys41 is thought to enhance catalysis by stabilizing the transition state through the H-bond interaction between the side-chain H^{ζ} of Lys41 and the oxygen atom of P−O.[37] Except for the three catalytically important residues, Gln11 of RNase A is also known as an important residue in the P_1 site and it is also thought to enhance catalysis by stabilizing the transition state through H-bond,[38] similar to Lys41. Recently, the properties of the side-chain conformations of His12 and His119 have been well characterized based on six high resolution X-ray crystal structures determined at different pH values.[39,40] It has been found that the His12 side-chain is not influenced by change of pH and shows very low mobility. In contrast, His119, unlike His12, shows high mobility and has two alternative conformations, referred to as A and B. Both A and B conformations occur at acidic pH, while only the A conformation occurs at basic pH. The equivalent residues of the P_1 subsite are Lys9, His10, Lys31, and His98 in rRNase 4, and Lys9, His10, Lys31 and His97 in ONC.

Comparisons of the side-chain conformations of the residues in each subsite of RNase A and of their equivalent residues in rRNase 4 and ONC are shown in Figure 6(b). These clearly reveal that the side-chain conformation of His98 of rRNase 4 as well as His97 of ONC is different from the conformation of the A form of His112 in RNase A. On the contrary, His98 side-chain conformation resembles the B form conformation (plot not shown) and shows a low mobility with the RMSD of 1.12 Å. This side-chain conformational difference might be one of the key factors why RNase A possesses much higher catalytic activity than frog ribonucleases. In addition, we found that the side-chain conformations of Lys9 and His10 of rRNase 4 are different from those of ONC. Both structures of rRNase 4 and ONC were determined at acidic conditions (pH 3.5 for rRNase 4 and pH 4.5 for ONC[27]). The protonation state of the catalytic His and Lys residues should be the same at pH 3.5 and 4.5, indicating that it is unlikely that the side-chain conformation at the P_1 site would change at this pH range. Therefore, the conformation difference of Lys9 and His10 observed in rRNase 4 and ONC should be due to other factors. As described above, there is a H-bond interaction between the side-chain H^{ε} of Lys9 and the side-chain carbonyl oxygen of N-terminal pyroglutamate in ONC, but this H-bond is not present in rRNase 4. We propose that the loss of this H-bond in rRNase 4 is the key factor that causes the different side-chain conformations in Lys9 and His10 residues between rRNase 4 and ONC. To further confirm this assumption, we generated the structure of native RNase 4 using rRNase 4 structure as a template since there is no significant change in the NMR parameters, especially NOEs, between rRNase 4 and RNase 4. Interestingly, the side-chain conformations of the P_1 site residues in RNase 4 are much similar to those of ONC, indicating that the extra Met residue and the replacement of pyroglutamate by glutamine in the N terminus of rRNase 4 would render side-chain conformational changes in the P_1 active site. It is possible that the orientations of the catalytic residues of rRNase 4 are not optimal for cleavage of the substrates and responsible for the dramatic decrease in the catalytic activity for rRNase 4.

For base preference, four residues (Thr45, Asp83, Phe120, and Ser123) are involved in the B_1 subsite of RNase A. The equivalent residue of Asp83 is Glu67 in rRNase 4 and Asp67 in ONC. Both RNase A and ONC have the base preference of uridine in the B_1 site, but RNase 4 has a base preference of cytosine. Therefore, we suggest that replacement of the Asp residue with a Glu residue is the main factor that contributes to the change in the B_1 base preference between ONC and RNase 4. A comparison of the side-chain conformations of the B_1 site residues among RNase A, ONC, and rRNase 4 showed that the side-chain conformation of Glu67 in rRNase 4 is different from that of RNase A and ONC, further supporting our suggestion that the conversion of the Asp residue into Glu causes the change in the B_1 base preference for RNase 4. The B_2 base preference of RNase A is adenine, different from guanine in rRNase 4 and ONC. The B_2 subsite of RNase A contains Asn67, Gln69, Asn71, and Glu111. The corresponding residues of Glu111 are conserved, Glu92 in rRNase 4 and Glu91 in ONC, indicating that they might also play an important role in the B_2 subsite. However, the other three residues (Asn67, Gln69, and Asn71) are located within the loop region and this loop conformation is dramatically different from that of the equivalent region of rRNase 4 and ONC. Therefore, we suspect that some other residues, in addition to Glu92, are involved in the recognition of the B_2 base (guanine) in rRNase 4.

In summary, we found that the unusual chemical shifts observed in rRNase 4 are closely associated with its structure. Most interestingly, based on a comparison of the available tertiary structures in the RNase A superfamily, along with our NMR studies involving frog ribonucleases, we conclude that most of these unusual chemical shifts are common features and are likely to be found in other members in the RNase A superfamily, although they exhibit different biological functions. Knowing these unusual chemical shift properties would be helpful in future NMR structural studies involving RNase A superfamily proteins. We also found that rRNase 4 possesses a tertiary structure similar to the native protein, and that the loss of two H-bonds in the N-terminal glutamate is one of the important factors contributing to the drastic reduction of the biological functions in rRNase 4.

Materials and Methods

Preparation of ribonucleases

RNase A was purchased from Roche (Roche Molecular Biochemicals, Mannheim, Germany). RC-RNase and RNase 4 were purified from *R. catesbeiana* (bullfrog) oocytes as described.[1] The uniformly ^{15}N or ^{13}C-labeled rRNase 4 with an extra Met at its N terminus was produced in *Escherichia coli* BL21 (DE3) from the rRNase 4 gene[1] cloned in pET-22b (Novagen), induced by isopropyl-β-thiogalactopyranoside (IPTG). The inclusion bodies were collected after the cells were lyzed by microfluidizer and resolved in 6 M GdnHCl at room temperature for one hour. The proteins were then rapidly diluted to a final protein concentration of 70 μg/ml with a solution of Tris-acetate buffer (pH 8.5), containing 0.5 M L-arginine, 3 mM reduced glutathione, and 0.6 mM oxidized glutathione, and incubated at 10 °C for 24 hours.[5] The refolding solution was concentrated and dialyzed against sodium acetate (pH 5.0), followed by carboxymethyl cellulose (CM52, Whatman) and FPLC mono S (Pharmacia) column chromatography. SDS-electrophoresis and ES/MS spectrometry were carried out to confirm the derived proteins.

Ribonuclease activity assay

Ribonuclease activities were analyzed by zymogram assay on RNA-casting PAGE.[41] Briefly, after electrophoresis the gel was washed twice with 25% (v/v) isopropyl alcohol in 10 mM Tris–HCl (pH 7.5), to remove SDS for protein renaturation. The activity was observed after incubating the gel at room temperature for 30 minutes in 10 mM Tris–HCl (pH 7.5), followed by 0.2% (w/v) Toluidine blue O staining. In addition, the ribonuclease activity of each purified ribonuclease was also determined by the release of acid-soluble nucleotides from bakers' yeast total RNA after ribonuclease digestion in 50 mM sodium acetate (pH 6.0). The specific activity of the enzyme was defined as the increase of absorbance at 260 nm by 1 μg ribonuclease at 37 °C for 15 minutes.[41] The specific cleavage sites on RNA were determined by incubation of ribonucleases with 5′-^{32}P-labeled 18-mer RNA with the sequence, 5′-AAGGUU AUCCGCACUGAA-3′, followed by denaturing gel electrophoresis and autoradiography.[42] The k_{cat}/K_m of ribonucleases toward dinucleotide CpG and UpG was performed as follows. Briefly, dinucleotides were digested with ribonucleases at 37 °C for ten minutes in buffer containing 100 mM Mes (pH 6.0), 50 mM NaCl, 0.1 mg/ml bovine serum albumin and separated by reverse-phase HPLC using 1–5% acetonitrile (depended on products) in 0.1% TFA on a column of Vydac C18 with a Waters automated gradient controller.[41]

Assay of cytotoxicity by ATP Lite-M measurement

ATP is a marker for cell viability because it is present in all metabolically active cells. Its concentration declines very rapidly when cells undergo necrosis or apoptosis. The ATP Lite-M assay system (Packard BioScience Company, the Netherlands) is based on the production of light caused by the reaction of ATP with added luciferase and D-luciferin. The emitted light is proportional to the ATP concentration and was counted by a Packard Top Count Microplate Scintillation and Luminescence Counter. Briefly, HeLa cells (5×10^3) in 96-well plates in 100 μl Dulbecco's modified Eagle's medium (DMEM) were lyzed with 50 μl lysis buffer for two minutes followed by the addition of 50 μl substrate solution for one minute, then transferred to a dark adapt plate for ten minutes before luminescence counting.[1]

Assay of conformational stability

Ultra pure GdnHCl was purchased from Gibco BRL (Grand Island, NY) and used without further purification. All other chemicals were of reagent grade. CD experiments were carried out using an Aviv 202 SF CD spectrometer (Lakewood, NJ) calibrated with (+)-10-camphorsulfonic acid (CSA) at 25 °C. In general, a 2 mm path-length cuvette with 20 μM RNase 4 or rRNase 4 in 20 mM phosphate was used for CD experiments and all the protein solutions were made up to 1 ml. The CD spectra at different temperatures and pH values were recorded. All CD data were obtained from an average of three scans with 1 nm bandwidth. The spectra were recorded from 180 nm to 260 nm, at a scanning rate of 38 nm/minute with a wavelength step of 0.5 nm and time constant of 100 ms. After background subtraction and smoothing, all the CD data were converted from CD signal (millidegree) into mean residue ellipticity (deg cm^2 dmol^{-1}). The secondary structure content was estimated from the CD spectra according to the methods of CONTIN, SELCON and CDSSTR.[43] Equilibrium thermo-denaturing experiments were performed by measurement of the change of molar ellipticity at 228 nm. Data were collected as a function of temperature with a scan rate of 2 deg. C/minute over a range of 20–95 °C in 20 mM phosphate buffer (pH 3.0). The variation was monitored at 228 nm after three minutes equilibration at each point with a temperature controller. Equilibrium unfolding induced by GdnHCl was monitored by steady-state far-UV CD. RNase 4 (10 μM) in 20 mM phosphate buffer (pH 3.0), was mixed with varying amounts of RNase 4 (10 μM) in 8 M GdnHCl (pH 3.0), in a Microlab titrator (Hamilton) to yield the desired final GdnHCl concentrations, and changes of ellipticity at 228 nm were followed.

NMR spectroscopy

All NMR experiments were performed on a Bruker AVANCE 600 spectrometer equipped with a triple (^{1}H, ^{13}C and ^{15}N) resonance probe including a shielded *z*-gradient. NMR samples were prepared in 50 mM phosphate buffer in 90% H_2O/10% ^2H_2O at pH 3.5, 310 K and contained 0.35 ml of 1.5 mM protein in a Shigemi NMR tube. For the RNase 4, 2D ^{1}H NMR spectra (COSY, TOCSY and NOESY) were collected. All heteronuclear NMR experiments for rRNase 4 were carried out as described in the review article.[44] All spectra were processed using XWIN-NMR and analyzed using AURELIA on an SGI O_2 workstation. Linear prediction was used in the ^{13}C and ^{15}N dimensions to improve the digital resolution.

Torsional angle restraints and stereospecific assignment

The $^3J_{NH\alpha}$ coupling constants were estimated from the residual intensity of the antiphase cross-peak in DQF-COSY spectra recorded in H_2O. ϕ Torsional restraints of $-130(\pm 30)°$ for $^3J_{NH\alpha}$ coupling constants greater than 8 Hz, and $-60(\pm 30)°$ for $^3J_{NH\alpha}$ coupling constants smaller than 6 Hz, were used for structure calculation. In addition, we also used the TALOS program[45] to calculate the backbone ϕ, ψ torsion angles. The ϕ, ψ torsional restraints were used for structure generations starting from the early stage when NOE correlations were also consistent. The stereospecific assignments were derived from the method of Hyberts *et al.*[46] The $^3J_{\alpha\beta}$ and $^3J_{\alpha\beta'}$ coupling constants were estimated as either large or small based on: (a) the intensities of the cross-peaks observed in a DQF-COSY spectrum in ^2H_2O and a TOCSY spectrum recorded in short mixing time, and (b) the relative intensities of the intra-residue $C^\alpha H–C^\beta H$ and $NH–C^\beta H$ NOE cross-peaks. The stereospecific assignment of β-methylene also allowed us to assign the χ_1 torsion angle restraints to either $60(\pm 30)°$, $180(\pm 30)°$, or $-60(\pm 30)°$. In order to ensure the accuracy of stereospecific assignments, we obtained 23 prochiral assignments with certainty. We found that the stereospecific assignments agreed well with our generated structures in the early stage. Thus, in the later stage of structure generation, we also added χ_1 and prochiral assignments as restraints in the structure calculation.

Hydrogen bond and disulfide restraints

The amide-proton exchange rates were identified from residual amide proton signals observed in several 2D

TOCSY and $^{1}H-^{15}N$ HSQC spectra recorded at 310 K and pH 3.5 in $^{2}H_2O$. The amide proton exchange rates were categorized into three classes, fast, medium, and slow exchange rates. Hydrogen bond formation or solvent exclusion from the amide protons was assumed to account for the slow and medium exchange rate amide protons. For better convergence, a number of hydrogen bonds involved in the secondary structure were included as distance restraints in the final stage of structure generation, i.e. an O–N distance of 2.5–3.3 Å, and an O–HN distance of 1.8–2.5 Å were assigned in the latter stage of structure determination to the slow and medium exchanging protons, respectively. In the final stage of structure calculation, the hydrogen bonds between NH_i and OC_j in the β-sheet structures were included as restraints only if the β-sheet inter-strand NH_i/NH_j, $NH_i/C_\alpha H_{j+1}$, and $C_\alpha H_{i-1}/C_\alpha H_{j+1}$ NOE cross-peaks were observed. The disulfide bonds used in the structure calculation were Cys19 to Cys68, Cys30 to Cys76, Cys48 to Cys91, and Cys88 to Cys105. Covalent bonds between the sulfur atoms of disulfide bridges were modeled by restraining the distances between the two sulfur atoms to 1.80–2.30 Å.

Tertiary structure calculations

Distance restraints of rRNase 4 were derived primarily from the 100 and/or 200 ms 3D NOESY-HSQC spectra recorded in the aqueous solution at 310 K and pH 3.5. Peak intensities were classified as large, medium, small, and very small, corresponding to upper bound inter-proton distance restraints of 2.5 Å, 3.5 Å, 4.5 Å, and 6.0 Å, respectively. An additional correction of 1.0 Å was added for methylene and methyl groups. A set of 1323 restraints was applied for simulated annealing and energy minimization calculations using the program X-PLOR 98[47] on a SGI O_2 workstation. The INSIGHT II (Molecular Simulation Inc., San Diego, CA), MOLMOL,[48] and GRASP[49] programs were used to visually observe sets of structures and to calculate and make the electrostatic surface potential of the final three-dimensional models. The distributions of the backbone dihedral angles of the final converged structures were evaluated by the representation of the Ramachandran dihedral pattern, indicating the deviations from the sterically allowed (ϕ, ψ) angle limits using PROCHECK-NMR.[50]

Data Bank accession number

The chemical shifts of rRNase 4 at pH 3.5 and 310 K have been deposited to BioMagResBank under accession number BMRB-4893. The atomic coordinates of the 15 energy-minimized conformers used to represent the solution structure of rRNase 4 have been deposited in the Brookhaven Protein Data Bank, together with the complete list of conformational restraints used for the structure calculation under accession number 1 KVZ.

Acknowledgements

This work was supported by the National Science Council (NSC 90-2311-B-001-150) to C.C. and (NSC 89-2311-B-001-083) to Y.D.L., and by Academia Sinica, Taipei, Taiwan, ROC. We thank Dr Victor Lee Weaver for critical reading of the manuscript and Dr Yuan-Chao Lou for acquiring CD spectra at different pH values.

References

1. Liao, Y. D., Huang, H. C., Leu, Y. J., Wei, C. W., Tang, P. C. & Wang, S. C. (2000). Purification and cloning of cytotoxic ribonucleases from *Rana catesbeiana* (bullfrog). *Nucl. Acids Res.* **28**, 4097–4104.
2. Rosenberg, H. F., Zhang, J., Liao, Y. D. & Dyer, K. D. (2001). Rapid diversification of RNase A superfamily ribonucleases from the bullfrog *Rana catesbeiana*. *J. Mol. Evol.* **53**, 31–38.
3. Darzynkiewicz, Z., Carter, S. P., Mikulski, S. M., Ardelt, W. J. & Shogen, K. (1988). Cytostatic and cytotoxic effects of Pannon (P-30 Protein), a novel anticancer agent. *Cell Tissue Kinet.* **21**, 169–182.
4. Juan, G., Ardelt, B., Li, X., Mikulski, S. M., Shogen, K., Ardelt, W. *et al.* (1998). G1 arrest of U937 cells by onconase is associated with suppression of cyclin D3 expression, induction of p16INK4A, p21WAF1/CIP1 and p27KIP and decreased pRb phosphorylation. *Leukemia*, **12**, 1241–1248.
5. Boix, E., Wu, Y., Vasandani, V. M., Saxena, S. K., Ardelt, W., Ladner, J. & Youle, R. J. (1996). Role of the N terminus in RNase A homologues: differences in catalytic activity, ribonuclease inhibitor interaction and cytotoxicity. *J. Mol. Biol.* **257**, 992–1007.
6. Shapiro, R., Harper, J. W., Fox, E. A., Jansen, H. W., Hein, F. & Uhlmann, E. (1988). Expression of Met-(−1) angiogenin in *Escherichia coli*: conversion to the authentic less than Glu-1 protein. *Anal. Biochem.* **175**, 450–461.
7. Leland, P. A., Schultz, L. W., Kim, B. M. & Raines, R. T. (1998). Ribonuclease A variants with potent cytotoxic activity. *Proc. Natl Acad. Sci. USA*, **95**, 10407–10412.
8. Klink, T. A. & Raines, R. T. (2000). Conformational stability is a determinant of ribonuclease A cytotoxicity. *J. Biol. Chem.* **275**, 17463–17467.
9. Notomista, E., Catanzano, F., Graziano, G., Dal Piaz, F., Barone, G., D'Alessio, G. & Di Donato, A. (2000). Onconase: an unusually stable protein. *Biochemistry*, **39**, 8711–8718.
10. Wu, Y., Mikulski, S. M., Ardelt, W., Rybak, S. M. & Youle, R. J. (1993). A cytotoxic ribonuclease. Study of the mechanism of onconase cytotoxicity. *J. Biol. Chem.* **268**, 10686–10693.
11. Laccetti, P., Portella, G., Mastronicola, M. R., Russo, A., Piccoli, R., D'Alessio, G. & Vecchio, G. (1992). *In vivo* and *in vitro* growth-inhibitory effect of bovine seminal ribonuclease on a system of rat thyroid epithelial transformed cells and tumors. *Cancer Res.* **52**, 4582–4586.
12. Kobe, B. & Deisenhofer, J. (1995). A structural basis of the interactions between leucine-rich repeats and protein ligands. *Nature*, **374**, 183–186.
13. Leland, P. A., Staniszewski, K. E., Kim, B. M. & Raines, R. T. (2001). Endowing human pancreatic ribonuclease with toxicity for cancer cells. *J. Biol. Chem.* **276**, 43095–43102.
14. Campbell, R. L. & Petsko, G. A. (1987). Ribonuclease structure and catalysis: crystal structure of sulfate-free native ribonuclease A at 1.5-Å resolution. *Biochemistry*, **26**, 8579–8584.
15. Fontecilla-Camps, J. C., de Llorens, R., le Du, M. H. & Cuchillo, C. M. (1994). Crystal structure of ribonuclease A.d($A_pT_pA_pA_pG$) complex. Direct evidence

for extended substrate recognition. *J. Biol. Chem.* **269**, 21526–21531.
16. Leonidas, D. D., Hapiro, R., Irons, L. I., Russo, N. & Acharya, K. R. (1997). Crystal structures of ribonuclease A complexes with 5′-diphosphoadenosine 3′-phosphate and 5′-diphosphoadenosine 2′-phosphate at 1.7 Å resolution. *Biochemistry*, **36**, 5578–5588.
17. Aguilar, C. F., Thomas, P. J., Moss, D. S., Mills, A. & Palmer, R. A. (1991). Novel non-productively bound ribonuclease inhibitor complexes—high resolution X-ray refinement studies on the binding of RNase-A to cytidylyl-2′,5′-guanosine (2′,5′CpG) and deoxycytidylyl-3′,5′-guanosine (3′,5′dCpdG). *Biochim. Biophys. Acta*, **1118**, 6–20.
18. Santoro, J., Gonzalez, C., Bruix, M., Neira, J. L., Nieto, J. L., Herranz, J. & Rico, M. (1993). High-resolution three-dimensional structure of ribonuclease A in solution by nuclear magnetic resonance spectroscopy. *J. Mol. Biol.* **229**, 722–734.
19. Toiron, C., Gonzalez, C., Bruix, M. & Rico, M. (1996). Three-dimensional structure of the complexes of ribonuclease A with 2′,5′-CpA and 3′,5′-d(CpA) in aqueous solution, as obtained by NMR and restrained molecular dynamics. *Protein Sci.* **5**, 1633–1647.
20. Pous, J., Mallorqui-Fernandez, G., Peracaula, R., Terzyan, S. S., Futami, J., Tada, H. *et al.* (2001). Three-dimensional structure of human RNase 1 delta N7 at 1.9 Å resolution. *Acta Cryst. D* **57**, 498–505.
21. Mosimann, S. C., Newton, D. L., Youle, R. J. & James, M. N. (1996). X-ray crystallographic structure of recombinant eosinophil-derived neurotoxin at 1.83 Å resolution. *J. Mol. Biol.* **260**, 540–552.
22. Boix, E., Leonidas, D. D., Nikolovski, Z., Nogues, M. V., Cuchillo, C. M. & Acharya, K. R. (1999). Crystal structure of eosinophil cationic protein at 2.4 Å resolution. *Biochemistry*, **38**, 16794–16801.
23. Mallorqui-Fernandez, G., Pous, J., Peracaula, R., Aymami, J., Maeda, T., Tada, H. *et al.* (2000). Three-dimensional crystal structure of human eosinophil cationic protein (RNase 3) at 1.75 Å resolution. *J. Mol. Biol.* **300**, 1297–1307.
24. Terzyan, S. S., Peracaula, R., de Llorens, R., Tsushima, Y., Yamada, H., Seno, M. *et al.* (1999). The three-dimensional structure of human RNase 4, unliganded and complexed with d(Up), reveals the basis for its uridine selectivity. *J. Mol. Biol.* **285**, 205–214.
25. Acharya, K. R., Shapiro, R., Allen, S. C., Riordan, J. F. & Vallee, B. L. (1994). Crystal structure of human angiogenin reveals the structural basis for its functional divergence from ribonuclease. *Proc. Natl Acad. Sci. USA*, **91**, 2915–2919.
26. Papageorgiou, A. C., Shapiro, R. & Acharya, K. R. (1997). Molecular recognition of human angiogenin by placental ribonuclease inhibitor—an X-ray crystallographic study at 2.0 Å resolution. *EMBO J.* **16**, 5162–5177.
27. Mosimann, S. C., Ardelt, W. & James, M. N. (1994). Refined 1.7 Å X-ray crystallographic structure of P-30 protein, an amphibian ribonuclease with anti-tumor activity. *J. Mol. Biol.* **236**, 1141–1153.
28. Chang, C. F., Chen, C., Chen, Y. C., Hom, K., Huang, R. F. & Huang, T. H. (1998). The solution structure of a cytotoxic ribonuclease from the oocytes of *Rana catesbeiana* (bullfrog). *J. Mol. Biol.* **283**, 231–244.
29. Hsu, C. H., Liao, Y. D., Wu, S. H. & Chen, C. (2001). ^{1}H, ^{13}C and ^{15}N resonance assignments and secondary structure of the cytotoxic protein RNase 4 from bullfrog *Rana catesbeiana* oocytes. *J. Biomol. NMR*, **20**, 93–94.
30. Eberhardt, E. S., Wittmayer, P. K., Templer, B. M. & Raines, R. T. (1996). Contribution of a tyrosine side chain to ribonuclease A catalysis and stability. *Protein Sci.* **5**, 1697–1703.
31. Hsu, C. H., Chen, L. W., Liao, Y. D., Wu, S. H. & Chen, C. (2001). ^{1}H, ^{15}N and ^{13}C resonance assignments and secondary structure determination of the RC-RNase 2 from oocytes of bullfrog *Rana catesbeiana*. *J. Biomol. NMR*, **19**, 87–88.
32. Su, N. Y., Liao, Y. D., Chang, C. F., Wang, I. & Chen, C. (2001). ^{1}H, ^{15}N and ^{13}C resonance assignments and secondary structure of the liver ribonuclease from bullfrog *Rana catesbeiana*. *J. Biomol. NMR*, **20**, 189–190.
33. Usher, D. A., Richardson, D. I., Jr & Eckstein, F. (1970). Absolute stereochemistry of the second step of ribonuclease action. *Nature*, **228**, 663–665.
34. Usher, D. A., Erenrich, E. S. & Eckstein, F. (1972). Geometry of the first step in the reaction of ribonuclease-A (in-line geometry-uridine2′,3′-cyclic thiophosphate-31P NMR). *Proc. Natl Acad. Sci. USA*, **69**, 115–118.
35. Pares, X., Nogues, M. V., De Lorens, R. & Cuchillo, C. M. (1991). Structure and function of ribonuclease A binding subsites. *Essays Biochem.* **26**, 89–103.
36. Nogues, M. V., Vilanova, M. & Cuchillo, C. M. (1995). Bovine pancreatic ribonuclease A as a model of an enzyme with multiple substrate binding sites. *Biochim. Biophys. Acta*, **1253**, 16–24.
37. Raines, R. T. (1998). Ribonuclease A. *Chem. Rev.* **98**, 1045–1066.
38. Wlodawer, A., Miller, M. & Sjolin, L. (1983). Active site of RNase: neutron diffraction study of a complex with uridine vanadate, a transition-state analog. *Proc. Natl Acad. Sci. USA*, **80**, 3628–3631.
39. Berisio, R., Lamzin, V. S., Sica, F., Wilson, K. S., Zagari, A. & Mazzarella, L. (1999). Protein titration in the crystal state. *J. Mol. Biol.* **292**, 845–854.
40. Berisio, R., Sica, F., Lamzin, V. S., Wilson, K. S., Zagari, A. & Mazzarella, L. (2002). Atomic resolution structures of ribonuclease A at six pH values. *Acta Crystallog. sect. D Biol. Crystallog.* **58**, 441–450.
41. Liao, Y. D. & Wang, J. J. (1994). Yolk granules are the major compartment for bullfrog (*Rana catesbeiana*) oocyte-specific ribonuclease. *Eur. J. Biochem.* **222**, 215–220.
42. Liao, Y. D. (1994). Determination of base specificity of multiple ribonucleases from crude samples. *Mol. Biol. Rep.* **20**, 149–154.
43. Sreerama, N. & Woody, R. W. (2000). Estimation of protein secondary structure from circular dichroism spectra: comparison of CONTIN, SELCON, and CDSSTR methods with an expanded reference set. *Anal. Biochem.* **287**, 252–260.
44. Kay, L. E. (1995). Pulsed field gradient multidimensional NMR methods for the study of protein structure and dynamics in solution. *Prog. Biophys. Mol. Biol.* **63**, 277–299.
45. Cornilescu, G., Delaglio, F. & Bax, A. (1999). Protein backbone angle restraints from searching a database for chemical shift and sequence homology. *J. Biomol. NMR*, **13**, 289–302.
46. Hyberts, S. G., Marki, W. & Wagner, G. (1987). Stereospecific assignments of side-chain protons and characterization of torsion angles in Eglin c. *Eur. J. Biochem.* **164**, 625–635.

47. Brunger, A. T. (1998). *X-PLOR Version 98*, Yale University Press, New Haven.
48. Koradi, R., Billeter, M. & Wuthrich, K. (1996). MOLMOL: a program for display and analysis of macromolecular structures. *J. Mol. Graph.* **14**, 29–32.
49. Nicholls, A., Sharp, K. A. & Honig, B. (1991). Protein folding and association: insights from the interfacial and thermodynamic properties of hydrocarbons. *Proteins*, **11**, 281–296.
50. Laskowski, R. A., Rullmannn, J. A., MacArthur, M. W., Kaptein, R. & Thornton, J. M. (1996). AQUA and PROCHECK-NMR: programs for checking the quality of protein structures solved by NMR. *J. Biomol. NMR*, **8**, 477–486.
51. Wlodawer, A., Svensson, L. A., Sjolin, L. & Gilliland, G. L. (1988). Structure of phosphate-free ribonuclease A refined at 1.26 Å. *Biochemistry*, **27**, 2705–2717.

Edited by M. F. Summers

(Received 23 September 2002; received in revised form 12 December 2002; accepted 12 December 2002)

Supplementary Material comprising one Table and three Figures is available on Science Direct